JMEPEG (2011) 20:1055–1062
DOI: 10.1007/s11665-010-9723-0

1059-9495/$19.00

Wear Characteristics and Mechanisms of H13 Steel with Various Tempered Structures

X.H. Cui, S.Q. Wang, M.X. Wei, and Z.R. Yang

(Submitted September 18, 2009; in revised form May 16, 2010)

Wear tests of H13 steel with various tempering microstructures were performed under atmospheric conditions at room temperature (RT), 200 °C, and 400 °C. The wear characteristics and wear mechanisms of various tempered microstructures of the steel were focused by investigating the structure, morphology, and composition of the worn surfaces. Under atmospheric conditions at RT, 200 °C, and 400 °C, adhesive wear, mild oxidation wear, and oxidation wear prevailed, respectively. The wear rate at 200 °C was substantially lower than those at RT and 400 °C due to the protection of tribo-oxides. In mild oxidation wear, the tempered microstructures of the steel presented almost no obvious influence on the wear resistance. However, in adhesive wear and oxidation wear, the wear resistance strongly depended on the tempered microstructures of the steel. The steel tempered at 600-650 °C presented pronouncedly lower wear rates than the one tempered at 200-550 or 700 °C. It can be suggested that the wear resistance of the steel was closely related with its fracture resistance.

Keywords heat treating, tool steel, tribology

1. Introduction

Hot working steels usually used for the die-forging tools are exposed to high thermal and mechanical stress. These stresses cause the failure of dies; the life of hot-forging dies is usually limited by complex interactive mechanisms under cyclic loading such as abrasive, adhesive and scaling wear, thermal and mechanical fatigue, and plastic deformation. The wear was reported to one of the predominant failure patterns due to friction between the die and the workpiece (Ref 1, 2). During hot working of the workpiece, the temperature of the die temporarily would exceed 500 °C, due to the fact that the temperature of forging pieces is well above 1000 °C (Ref 2). Therefore, hot working steels would experience further tempering under the high thermal and mechanical load. Barrau et al. (Ref 2) pointed out that the tempering effects on the steels caused a greater susceptibility to wear. Hence, the wear resistance of hot working steels closely relates with their tempering microstructures.

The microstructures of steels were found to have obvious influences on the wear resistance (Ref 3-10). Tyagi et al. (Ref 3) reported that the wear resistance linearly increased with increasing the martensite amount. Aksoy et al. (Ref 4) pointed out that martensite is a main factor deciding the wear resistance in the dual-phase steel. The wear resistance increased with increasing the hardness and amount of martensite. The influence of retained austenite on the wear performance of the steel was reported in the literature (Ref 5). Under the lower normal load, retained austenite slightly affected the wear resistance. As the normal load increased, retained austenite reduced the wear resistance. On the contrary, the wear resistance was increased with further increasing normal load. Wang et al. (Ref 6) studied the effects of microstructures on the wear performances of 52100 steel and 1080 steel. They reported that as a severe wear happened, the various microstructures presented obviously different wear performances. The wear resistance increased in a sequence as follows: martensite plus carbides, granular pearlite, martensite, bainite, lamellar pearlite. The second phases were also found to have an obvious influence on the wear resistance (Ref 7-10). However, the relation between the microstructures and the wear resistance had been not clarified, to date, due to the complicated service conditions.

The purpose of the present research is to clarify the wear characteristics and mechanism of H13 steel with various tempering microstructures under various ambient temperatures. H13 steel was heat-treated to have different tempered microstructures. The wear mechanisms of H13 steel with various tempering states were studied as a function of normal load through the analysis for structure, morphology, and composition of the worn surfaces. The relationship of wear resistance with the tempering microstructures was presented.

2. Experimental Procedure

The dry sliding wear tests were carried out under atmospheric conditions on a uni-directional pin-on-disk high-temperature wear tester (MG-200 type, made by Xuanhua Materials Testing Machine Factory, China). A commercial H13 steel was employed to fabricate pin samples with the dimension of $\Phi 6 \times 12$ mm. The pin samples were austenitized at 1040 °C for 20 min, oil quenched, and finally tempered at 200, 440,

X.H. Cui, S.Q. Wang, M.X. Wei, and **Z.R. Yang**, School of Materials Science and Engineering, Jiangsu University, Zhenjiang 212013, People's Republic of China. Contact e-mail: shuqi_wang@ujs.edu.cn.

Table 1 Chemical compositions of the tested steels

Steel	Element, wt.%							
	C	Cr	Mo	V	Si	Mn	S	P
H13	0.38	5.15	1.45	0.90	1.04	0.43	≤0.03	≤0.03
D2	1.51	11.52	0.42	0.21	0.026	0.32	≤0.03	≤0.03

500, 600, 650, and 700 °C to achieve various tempered microstrucutres. The disks with the dimension of $\Phi 70 \times 8$ mm were made from a commercial heat-treated D2 steel with a hardness of 58 HRC. The compositions of the pin and disk are shown in Table 1.

The wear tests for all the specimens adopted the following test parameters: room temperature (RT), 200 °C, 400 °C for ambient temperature; 150 N for normal load; 1 m/s for sliding speed, and 1.2×10^3 m for sliding distance. All the data of wear loss were measured from the pin samples. Prior to wear tests, the surfaces of the pins and disks were polished with 400-grit emery paper and degreased. The pin samples were cleaned with acetone, dried before and after the test, and then weighted the wear loss by a balance with an accuracy of 0.01 mg. Each data of wear loss was the average value of the three tests. The wear rate was calculated in terms of the formula: $Ws = \Delta W/d$, where ΔW is wear loss (mg) and d is sliding distance (m).

The morphology, composition, and structure of the worn surfaces were analyzed with a JSM-7001F type scanning electron microscope (SEM) equipped with Inca Energy 350 type energy-dispersive spectrum (EDS) and a D/Max-2500/pc type x-ray diffractometer (XRD), respectively. The hardness was measured with a HR-150A type Rockwell apparatus; the average hardness was attained by six-time repeated measurement for each specimen.

3. Results and Analysis

3.1 Microstructure and Hardness

The heat treatment dependence of microstructural evolution of H13 steel is well documented (Ref 11, 12). Martensite (α′) and a bit of retained austenite is achieved when the steel is austenitized at 1040 °C and oil cooled. Martensite is a solid solution of α-Fe with a supersaturated solution of carbon. With increasing tempering temperature, the solution of carbon in α′ reduced with a precipitation of supersaturated carbon in a successive form of transitional carbides (ε), cementite, and alloy carbides (Mo_2C, VC,Cr_7C_3, and $Cr_{23}C_6$) (Ref 11, 12).

The microstructural evolution of H13 steel under different tempering temperatures is summarized as follows. As the steel was tempered at 200 °C, tempered martensite was attained, as shown in Fig. 1(a). As the tempering temperatures were in the range of 440-650 °C, tempered troostite was achieved (Fig. 1b-e). As the tempering temperature reached 700 °C, tempered sorbite was achieved with the coarsened grains (Fig. 1f).

The hardness values of H13 steel as a function of the tempering temperature are shown in Fig. 2. The hardness would reduce with increasing the tempering temperature. It is clear that H13 steel with various tempering states presented the different hardness values or strengths. With increasing tempering temperature, the hardness first slightly decreased till 440 °C, then increased to the climax at 550 °C, and subsequently the hardness sharply reduced.

When the steel was tempered at 200 °C, the dispersed, fine ε-carbide was precipitated with a common lattice relationship with α′ (Ref 11, 12). Thus, tempered martensite was achieved to retain a high hardness. With further increasing the tempering temperature, the supersaturated carbon atoms continued to precipitate; the ε-carbide turned into cementite. Because the solid solubility of martensite reduced and the common lattice relationship of carbide with α′ lost, the hardness slightly reduced. As the steel was tempered at 440-500 °C,the dispersed alloy carbides (Mo_2C, VC, and Cr_7C_3) precipitated, which give high thermal stability and the coherent relation with α′ (Ref 11, 12). In this case, the secondary hardening appeared with an increase of hardness. As the tempering temperature reached the range of 550-650 °C, Cr_7C_3 as predominant carbide started to grow and the coherent relation with α′ lost (Ref 11, 12). Hence, the hardness sharply reduced. The microstructure for the steel tempered at 440-650 °C was tempered troostite. When tempering temperature was above 650 °C, tempered sorbite was achieved accompanied with Cr_7C_3 turning into $Cr_{23}C_6$. In this case, the steel started to recrystallize and $Cr_{23}C_6$ coarsened, thus the hardness further reduced (Ref 10).

3.2 Wear Performance

The wear rates of H13 steel tempered at various tempered temperatures under the different ambient temperatures are shown in Fig. 3. The wear rates at 200 °C presented almost no obvious influence of the tempering microstructures and were substantially lower than those at RT and 400 °C. However, the wear rates at RT and 400 °C strongly depended on the tempering microstructures.

Under atmospheric conditions at RT and 400 °C, their wear rates as a function of the tempering temperature presented almost the same regularity. As the tempering temperature was below 500 °C, the wear rates increased with increasing the tempering temperature. The samples tempered at 500 °C possessed the highest wear rate. As the tempering temperature surpassed 500 °C, the wear rate rapidly reduced. The samples tempered at 600 and 650 °C achieved the lower wear rates at RT and 400 °C, respectively. As tempering temperature further increased to 700 °C, the wear rate rapidly increased once more.

3.3 Structure, Morphology, and Composition of the Worn Surfaces

The XRD patterns for the worn surfaces of H13 steel tempered at 200, 600, and 700 °C under various ambient temperatures are shown in Fig. 4. At RT, only a bit of oxide appeared on the worn surfaces (Fig. 4a). At 200 °C, more Fe_3O_4 and less Fe_2O_3 existed as the predominant tribo-oxides (Fig. 4b). This meant that the worn surface started to obviously oxidize at 200 °C. As the ambient temperature reached 400 °C, the amount of tribo-oxides was pronouncedly increased with more Fe_3O_4, less Fe_2O_3, and a bit of FeO (Fig. 4c).

The morphology and composition of the worn surfaces under various ambient temperatures are shown in Fig. 5. In order to compare the variations of the compositions and structures after wear, the XRD pattern and EDS result of the pin specimens before wear tests are also represented in Fig. 6.

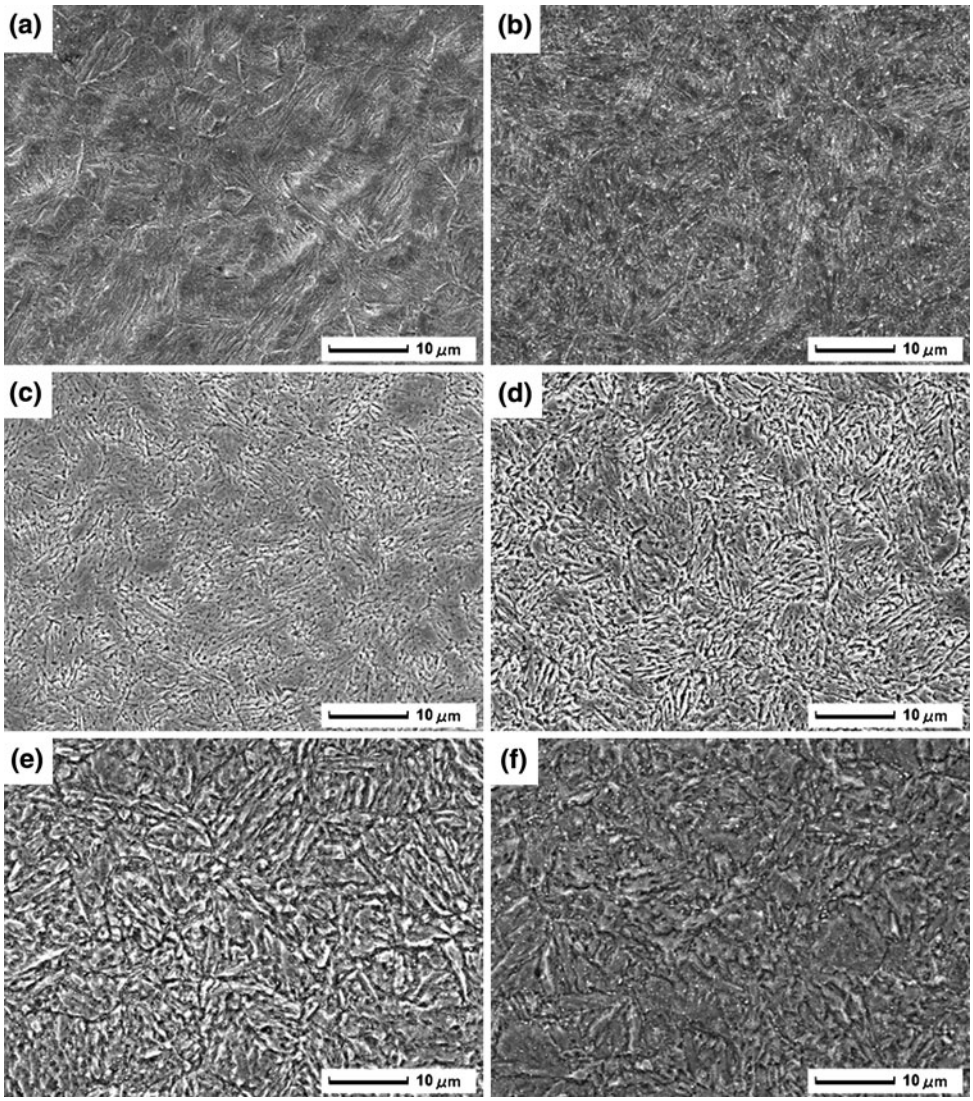

Fig. 1 Microstructures of H13 steel quenched at 1040 °C, tempered at 200 °C (a), 440 °C (b), 500 °C (c), 600 °C (d), 650 °C (e), and 700 °C (f)

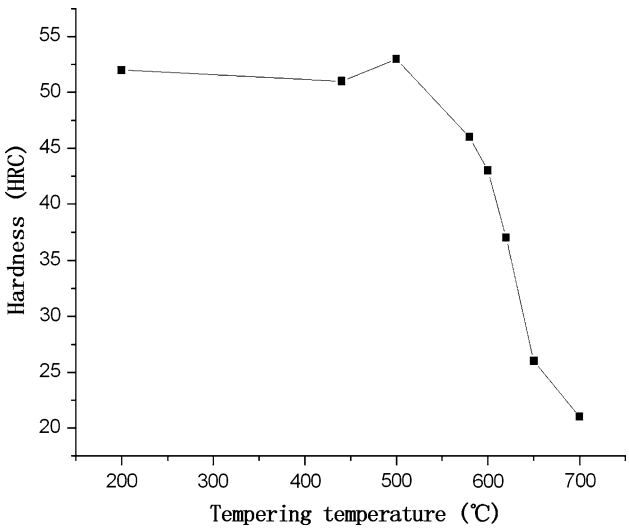

Fig. 2 Hardness of H13 steel as a function of tempered temperature

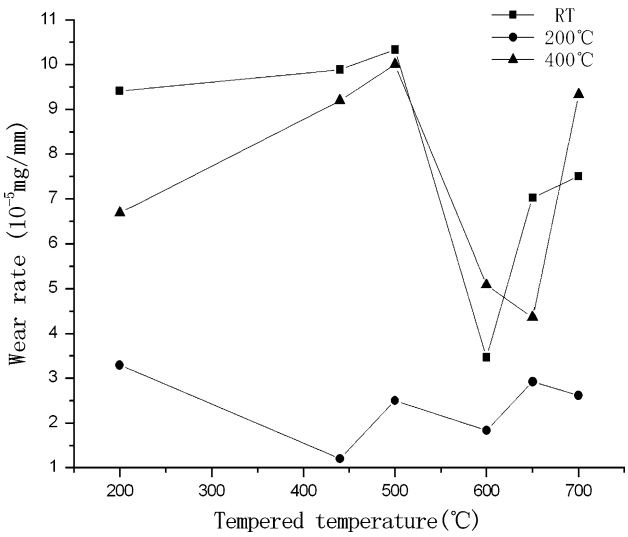

Fig. 3 Wear rates of H13 steel tempered at various tempered temperatures under different ambient temperatures

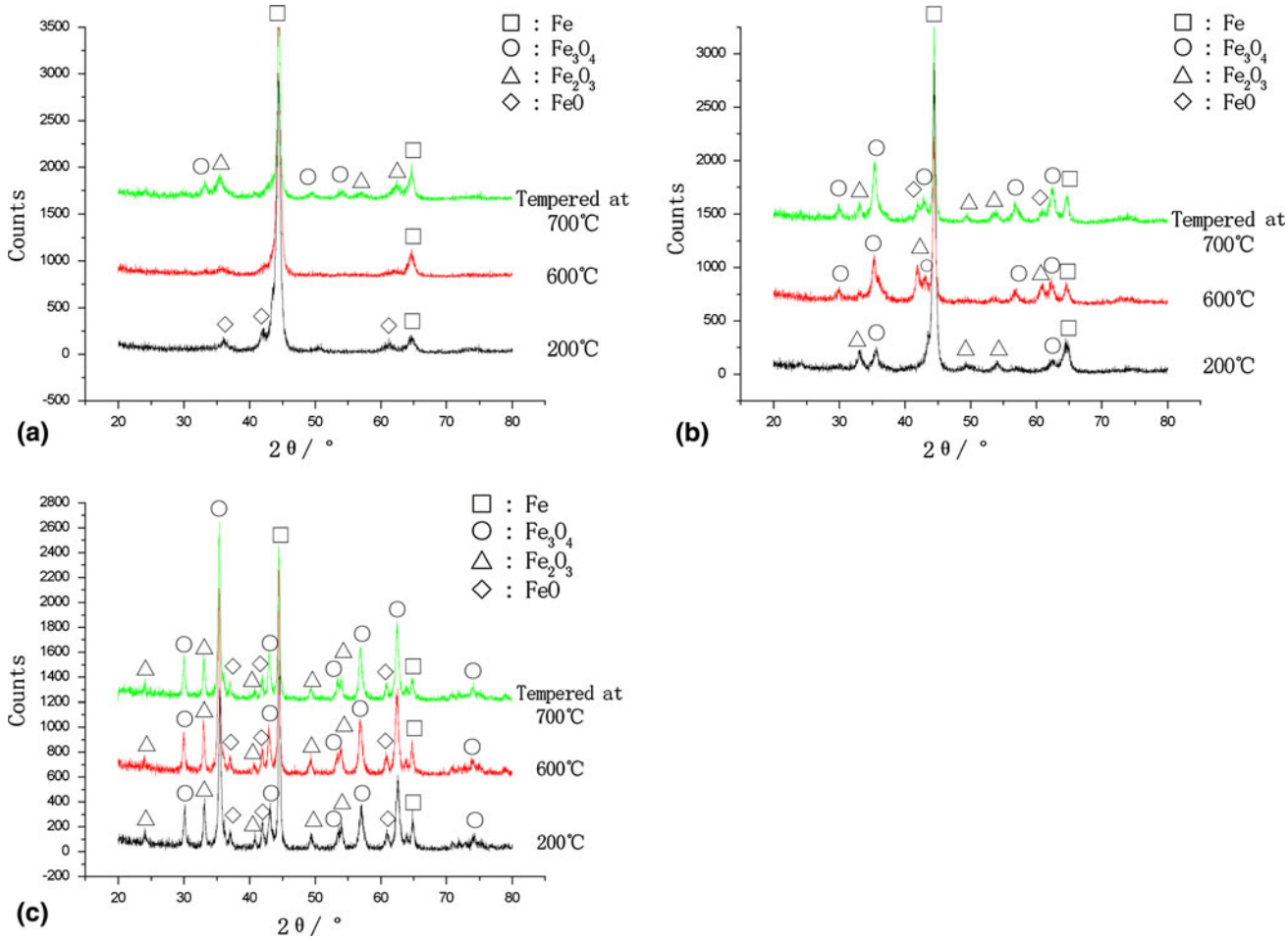

Fig. 4 XRD patterns of the worn surfaces for the specimens tempered at 200, 600, and 700 °C, respectively, under atmospheric conditions at RT (a), 200 °C (b), and 400 °C (c)

At RT, the typical adhesive traces presented on the worn surface, where there were more Fe and trace O (Fig. 5a, b). It is clear that adhesive wear was a predominant wear mechanism.

At 200 °C, a smooth, compact worn surface with some cracks and delamination regions was shown in Fig. 5(c). EDS analysis results showed an obviously high oxygen content on the worn surface (Fig. 5d). XRD patterns suggested that a layer of oxides formed on the worn surface (Fig. 4b).

As the ambient temperature reached 400 °C, many delamination regions appeared on the worn surface, where there was a high oxygen content (Fig. 5e, f). This meant that more oxides formed on the worn surfaces, which agreed with the XRD patterns (Fig. 4c). The more delamination regions gave an explanation for the high wear rate.

In order to further explore the wear mechanism, the section morphology of the worn surfaces was investigated. The section morphology of the worn surfaces under different ambient temperatures is shown in Fig. 7. Almost no oxide film could be found on the worn surface under the atmospheric conditions at RT (Fig. 7a). A layer of oxide film with a thickness of about 20 μm was produced on the worn surface under atmospheric conditions at 200 °C (Fig. 7b). Under atmospheric conditions at 400 °C, the formed oxide layer was relatively thin (about 10 μm) and tended to delaminate, as shown in Fig. 7(c).

4. Discussions

4.1 Wear Mechanisms Under Various Ambient Temperatures

The steels would react with oxygen to form an oxide layer on their surface because they are thermodynamically unstable in air. Hence, the high temperature and friction heat would readily result in the oxidation of steels under atmospheric conditions. The wear characteristics of steels under atmospheric conditions depends on the amount, thickness of tribo-oxides, and oxide-matrix bond (Ref 13, 14).

At RT, trace oxides were formed on the worn surfaces. The oxide layer was too thin to prevent from wear. This is a typical characteristic of adhesive wear, which belongs to severe wear. In this case, the wear performance depends on the matrix microstructures, and has no relation with tribo-oxides. At 200 and 400 °C, the amount of the tribo-oxide layer was enough to prevent wear to some extent. It is clear that the wear at 200 and 400 °C can be called oxidation wear. However, the oxidation wear at 200 °C is different from the one at 400 °C.

Oxidation wear was widely studied as mild oxidation wear, about which Quinn proposed a mild oxidation wear model (Ref 15, 16). As an oxide layer thickens until a critical thickness, it delaminates to cause wear loss. In this wear

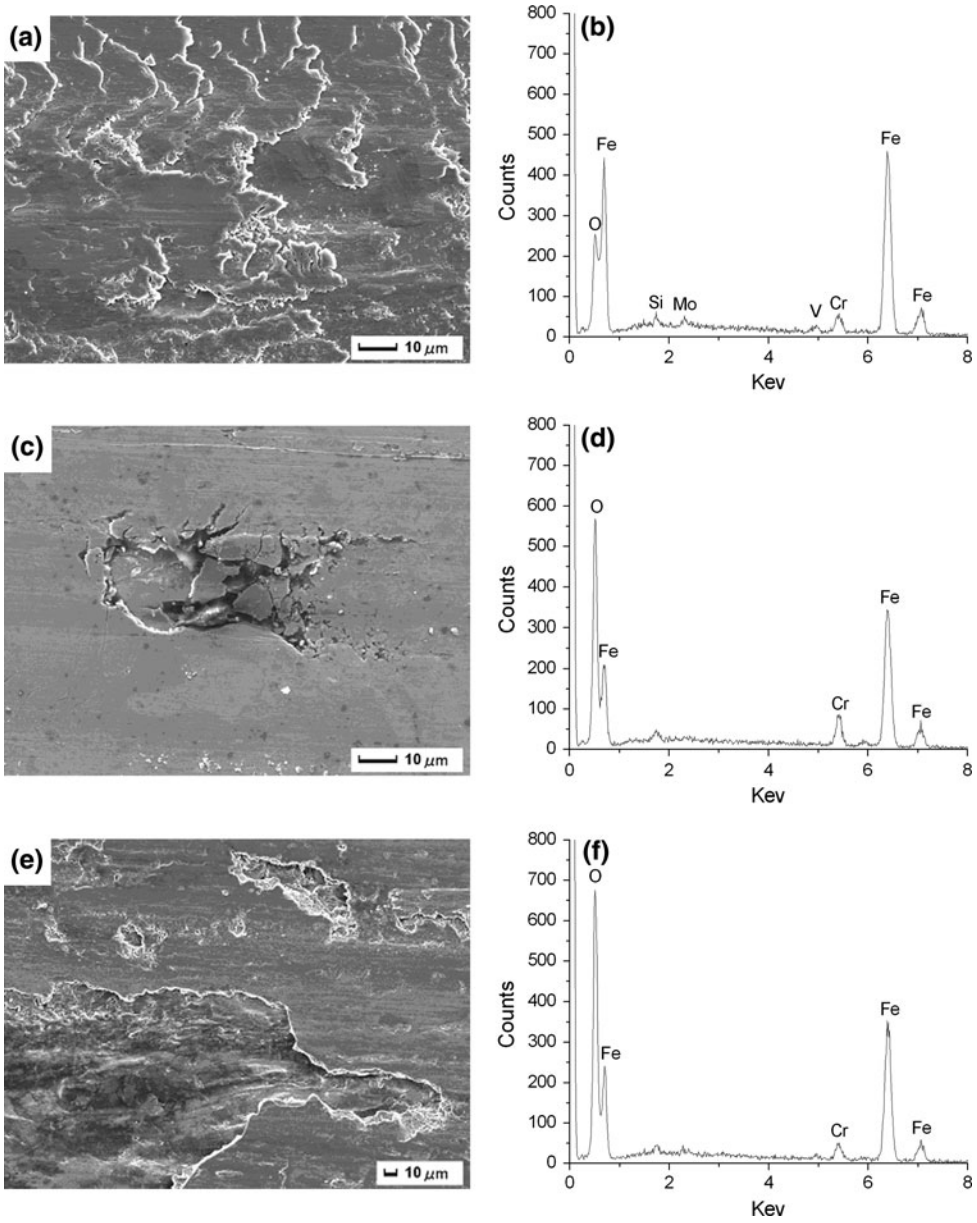

Fig. 5 Morphology and composition of the worn surfaces for the specimens tempered at 600 °C under the atmospheric conditions at RT (a, b), 200 °C (c, d), 400 °C (e, f)

regime, the wear behavior and wear rate only depend on the tribo-oxide layer, and nearly have no relation with the matrix structure (Ref 15-17). At 200 °C, the steel had enough strength to support the tribo-oxides that protect the steel from wear. In this case, the plastic deformation of the substrate underneath the tribo-oxides can be restricted. It is clear that the wear at 200 °C is a typical mild oxidation wear.

Oxidation wear and mild oxidation wear are different, but seldom clearly distinguished in the prior literature. In many researches, so-called oxidation wear may be not mild oxidation wear, which totally or partly beyond mild oxidation wear. In this case, the wear mechanism of the oxidation wear is different from mild oxidation wear. At 400 °C, high ambient temperature resulted in the high temperature on the worn surfaces, consequently softened the substrate beneath the tribo-oxides. Hence, the friction force resulted from higher normal load was liable to result in the apparent plastic deformation of matrix near the worn surfaces during wear. The steel was softened not to support the tribo-oxides, thus mild oxidation wear cannot be sustained. In this case, the wear loss would be increased with the transition of mild wear to severe wear. The tribo-oxide layer and the substrate microstructures would jointly function to affect the wear behavior and wear rate in the process of sliding (Ref 18). As a result, it can be suggested that the wear under atmospheric conditions at RT, 200 °C, and 400 °C is adhesive wear, mild oxidation wear, and oxidation wear, respectively.

4.2 Relation of Wear Resistance with Microstructures

It is clear that the substrate microstructures had obvious influence on wear performances at RT and 400 °C and slight or almost no influence on wear performances at 200 °C, as shown

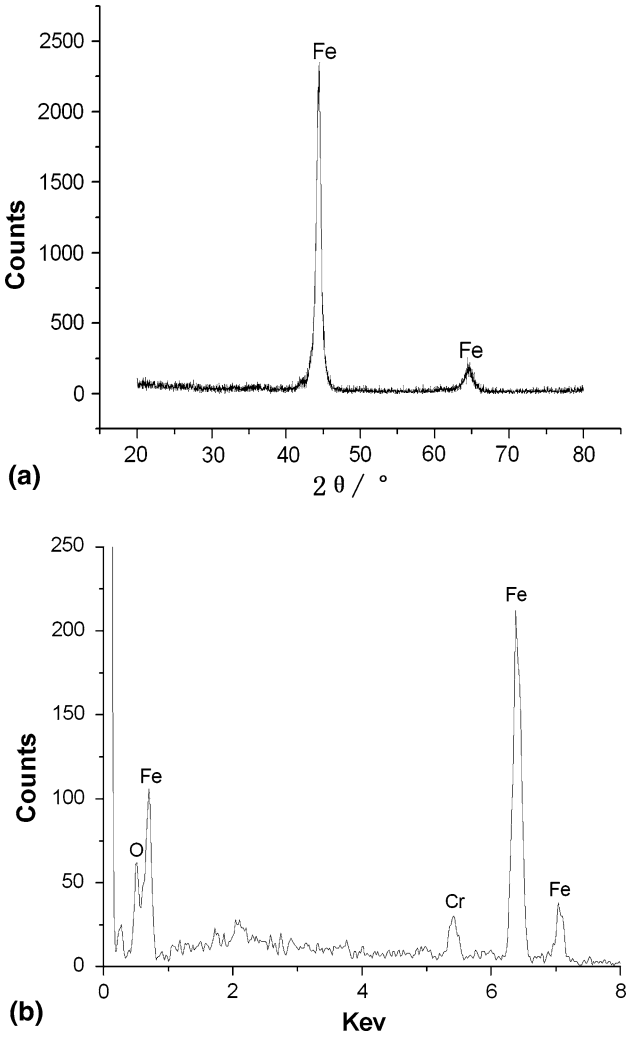

Fig. 6 XRD pattern (a) and EDS result (b) of the pin specimens tempered at 600 °C before wear

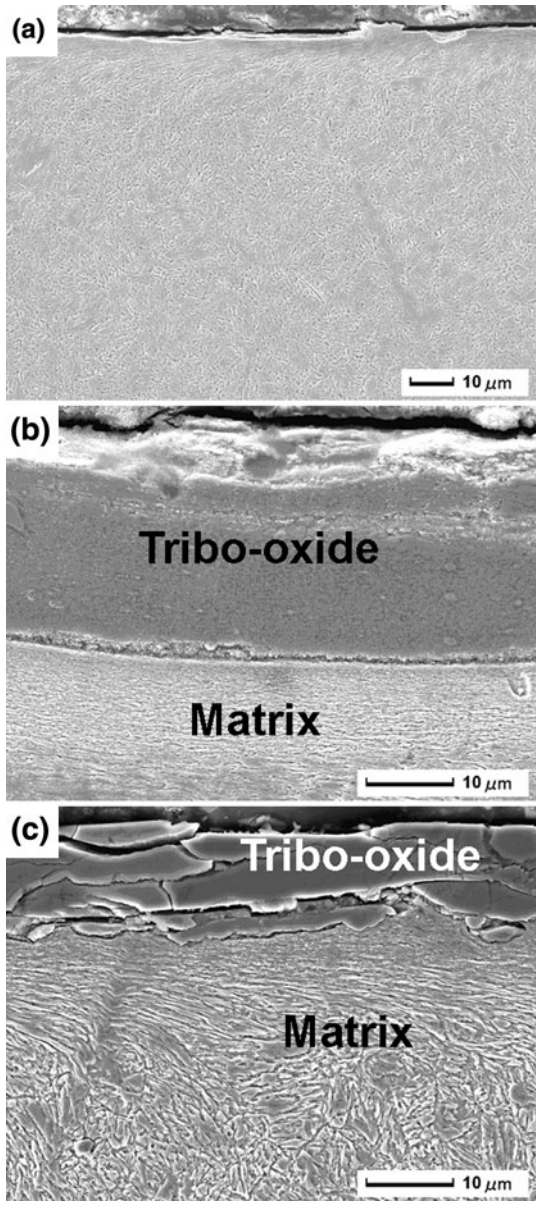

Fig. 7 Section morphology of worn surfaces for the specimens tempered at 600 °C under the atmospheric conditions at RT (a), 200 °C (b), and 400 °C (c)

in Fig. 3. It can be suggested that the wear resistance should have a close relation with the substrate microstructures in adhesive wear and oxidative wear. But mild oxidation wear did not present a corresponding relation between the substrate microstructures and the wear resistance.

In adhesive wear, the touching asperities stick together, subsequently sliding shear (deform), and finally pluck off (fracture) to result in the wear debris. In this case, the wear resistance should be closely related with the fracture resistance. The literature (Ref 11) reported that with increasing the tempering temperature, the impact toughness and fracture toughness of H13 steel first slightly increased, then rapidly reduced to the lowest point at 500 °C, and subsequently pronouncedly increased. The alloy carbides precipitated inside α′ and along the grain boundary after tempering at 500 °C, thus increasing hardness, but obviously reducing the fracture resistances with an inter-granular fracture (Ref 12). The above fracture resistances roughly correspond to the relation of the wear loss with the tempering temperature (Fig. 3). It is clear that the wear resistance is positively proportional to the fracture resistance. However, the totally corresponding relation between the wear resistance and the fracture toughness cannot be achieved due to different service conditions. Our above view is similar to the one of Wang et al. (Ref 6). They believed that wear resistance is positively proportional to energy consumption during wear.

In the oxidation wear, the delamination was reported to occur inside matrix under the elevated temperature and high load (Ref 19). In this process, cracks initiate, propagate in the matrix, and finally fractures to cause the wear loss. Hence, the wear loss also depends on the fracture resistance of steels. The section morphology of the worn surfaces under the wear at 400 °C is shown in Fig. 8. The different delamination patterns were found for the samples tempered at various temperatures.

The sample tempered at 200 °C presented high hardness, but relatively high brittleness (Ref 11). During wear, cracks would readily appear near worn surface. The oxygen would enter the matrix along the cracks and form oxides inside the cracks in the subsurface, as shown in Fig. 8(a) and (b).

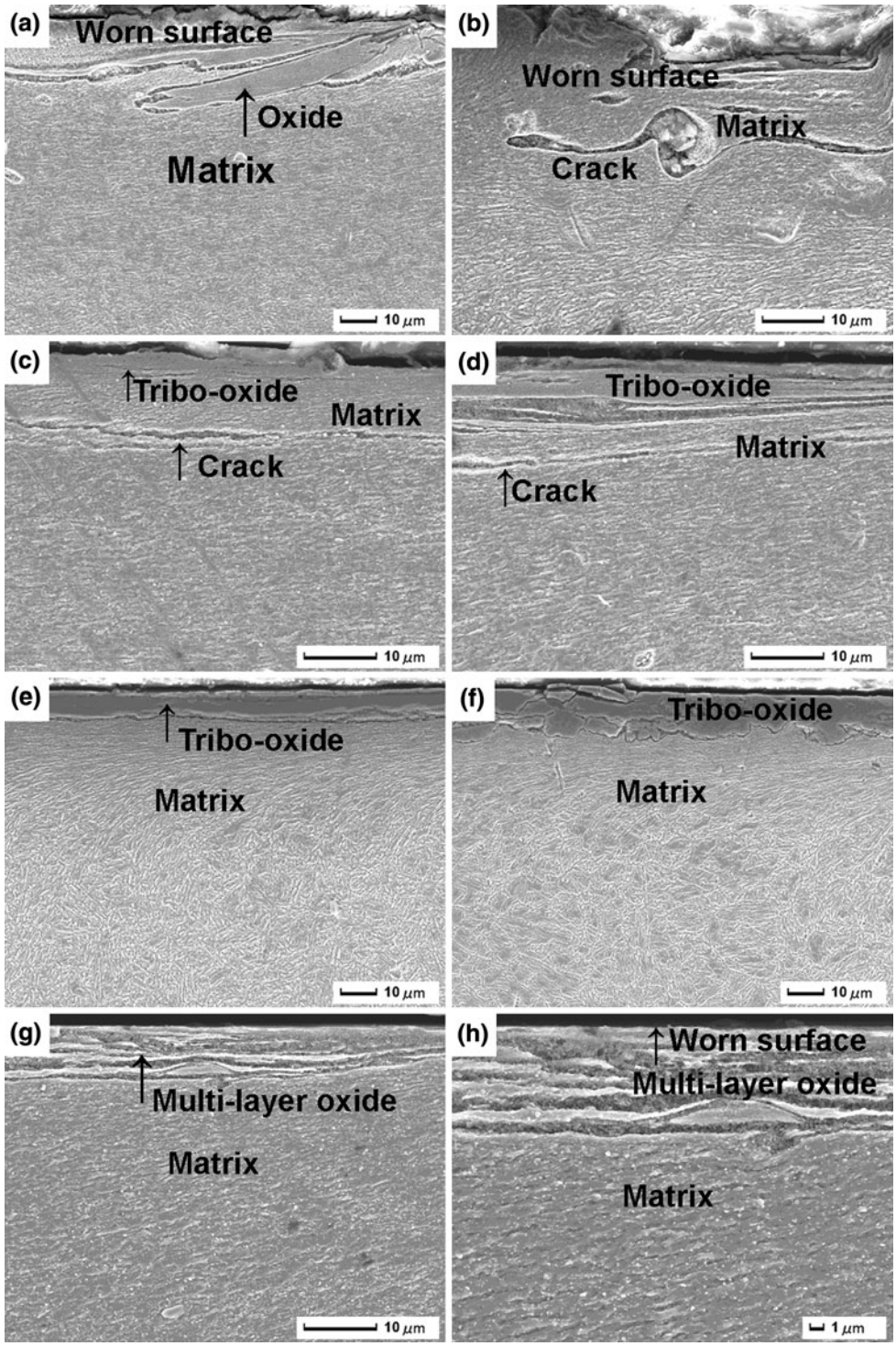

Fig. 8 Section morphology of the worn surfaces of H13 steel tempered at 200 °C (a, b), 440 °C (c), 500 °C (d), 600 °C (e), 650 °C (f), and 700 °C (g, h) under the atmospheric condition at 400 °C

Especially, cracks would initiate at the interface between the matrix and the oxide inside the matrix, propagate along the friction direction, and finally delaminate. In this case, the high wear rate would be achieved.

The sample tempered at 500 °C presented high hardness, but extremely high brittleness (Ref 11). In the severe plastic deformation region of the subsurface, the alloy carbides precipitated along the grain boundary would readily cause cracks initiating and propagating in matrix, and finally delaminating, as shown in Fig. 8(c) and (d). The wear loss would be the highest due to a great amount of brittle delamination.

The sample tempered at 600-650 °C has optimum strength and toughness (Ref 11). It had such a high fracture resistance that the cracks would not readily initiate in the matrix during wear. The section morphology presented the compact oxide

layer on the worn surfaces. The cracks and oxide inside the matrix were not observed, as shown in Fig. 8(e) and (f). In this case, oxide fatigue delamination from inside the oxides or the interface of the matrix and oxides results in low wear loss, thus the wear rate substantially reduced, compared with the delamination from matrix.

The sample tempered at 700 °C has low strength (21 HRC) and high ductility (Ref 11). Under the elevated temperature and high load, the steel did not support oxide layer on the worn surface. The massive plastic deformation occurred in the matrix near the worn surface. In addition, because friction heat cause the temperature near the worn surfaces to surpass the ambient temperature (400 °C). In this case, the pin sample was further tempered during wear. The precipitated carbide $Cr_{23}C_6$ would coarsen due to its low thermal stability (Ref 12). According to Suh's delamination theory, the coarse second phase would reduce bond between matrix and second phases. Under a load, in the plastically deformed subsurface, crack readily initiates and propagates at boundary between matrix and second phase (Ref 19). Hence, the multi-layer oxide readily appeared near the worn surface, as shown in Fig. 8(g) and (h). In this case, higher wear loss would be achieved.

5. Conclusions

The wear tests of H13 steel with various tempering states were performed under the atmospheric conditions at RT, 200 °C, and 400 °C. The following conclusions were drawn:

(1) Under atmospheric conditions at RT, 200 °C, and 400 °C, adhesive wear, mild oxidation wear, and oxidation wear prevailed, respectively.
(2) The wear rate at 200 °C was substantially lower than those at RT and 400 °C, due to the safeguard function of tribo-oxides. In the mild oxidation wear, the tempered temperatures of the steel presented slight or almost no obvious influence on the wear resistance.
(3) In adhesive wear and oxidation wear, the wear resistance strongly depended on the tempered microstructures of the steel. The steel tempered at 600-650 °C presented lower wear rates than the one tempered at 200-550 or 700 °C. It can be suggested that the wear resistance of the steel is closely related with its fracture resistance.

Acknowledgments

The authors gratefully acknowledge the financial supports of the advanced talent fund project from Jiangsu University (No. 07JDG062) and the nature science fund from Jiangsu Province (No. SBK2009221).

References

1. G.A. Fontalvo and C. Mitterer, The Effect of Oxide-Forming Alloying Elements on the High Temperature Wear of a Hot Work Steel, *Wear*, 2005, **258**(10), p 1491–1499
2. O. Barrau, C. Boher, R. Gras, and F. Rezai-Aria, Analysis of the Friction and Wear Behaviour of Hot Work Tool Steel for Forging, *Wear*, 2003, **255**(7–12), p 1444–1454
3. R. Tyagi, S.K. Nath, and S. Ray, Modelling of Dry Sliding Oxidation-Modified Wear in Two Phase Materials, *Wear*, 2003, **255**(1–6), p 327–332
4. M. Aksoy, M.B. Karamiş, and E. Evin, An Evaluation of the Wear Behaviour of a Dual-Phase Low-Carbon Steel, *Wear*, 1996, **193**(2), p 248–252
5. H.J. Kim and Y.G. Kweon, The Effects of Retained Austenite on Dry Sliding Wear Behavior of Carburized Steels, *Wear*, 1996, **193**(1), p 8–15
6. Y. Wang, T.C. Lei, and J.J. Liu, Tribo-Metallographic Behavior of High Carbon Steels in Dry Sliding: II. Microstructure and Wear, *Wear*, 1999, **231**(1), p 12–19
7. E. Marui, N. Hasegawa, H. Endo, K. Tanaka, and T. Hattori, Research on the Wear Characteristics of Hypereutectoid Steel, *Wear*, 1997, **205**(1–2), p 186–199
8. S.Q. Wang, F. Wang, X.H. Cui, and K.M. Chen, Effect of Secondary Carbides on Oxidation Wear of the Cr–Mo–V Cast Steels, *Mater. Lett.*, 2008, **62**(2), p 279–281
9. M. Vardavoulias, The Role of Hard Second Phases in the Mild Oxidational Wear Mechanism of High-Speed Steel-Based Materials, *Wear*, 1994, **173**(1–2), p 105–114
10. C. Rodenburg and W.M. Rainforth, A Quantitative Analysis of the Influence of Carbides Size Distributions on Wear Behaviour of High-Speed Steel in Dry Rolling/Sliding Contact, *Acta Mater.*, 2007, **55**(7), p 2443–2454
11. X.Z. Feng and S.W. Li, *Die Steels and Heat Treatment*, Mechanical Industry Press, Beijing, 1984, p 234 (in Chinese)
12. X.B. Hu, L. Lin, X.C. Wu, and M. Zhang, Coarsening Behavior of $M_{23}C_6$ Carbides After Ageing or Thermal Fatigue in AISI, H13 Steel with Niobium, *Int. J. Fatigue*, 2006, **28**(3), p 175–182
13. J. Jiang, F.H. Stott, and M.M. Stack, A Generic Model for Dry Sliding Wear of Metals at Elevated Temperatures, *Wear*, 2004, **256**(9–10), p 973–985
14. T.F.J. Quinn, J.L. Sullivan, and D.M. Rowson, Developments in the Oxidational Theory of Mild Wear, *Tribol. Int.*, 1980, **13**(4), p 153–158
15. T.F.J. Quinn, Oxidational Wear Modelling Part III. The Effects of Speed and Elevated Temperatures, *Wear*, 1998, **216**(2), p 262–275
16. J.E. Wilson, F.H. Stott, and G.C. Wood, The Development of Wear Protective Oxides and their Influence on Sliding Friction, *Proc. R. Soc.*, 1980, **369A**, p 557–574
17. H. So, D.S. Yu, and C.Y. Chuang, Formation and Wear Mechanism of Tribo-Oxides and the Regime of Oxidational Wear of Steel, *Wear*, 2002, **253**(9–10), p 1004–1015
18. S.Q. Wang, M.X. Wei, F. Wang, X.H. Cui, and C. Dong, Transition of Mild Wear to Severe Wear in Oxidative Wear of H21 Steel, *Tribol. Lett.*, 2008, **32**(2), p 67–72
19. X.H. Cui, S.Q. Wang, F. Wang, and K.M. Chen, Research on Oxidative Wear Mechanism of the Cast Steels, *Wear*, 2008, **265**(3–4), p 468–476